Atmospheric Measurement Techniques
Open Access
Discussions

Mixing layer height retrievals by multichannel microwave radiometer observations

D. Cimini[1,2], F. De Angelis[2], J.-C. Dupont[3], S. Pal[4,5], and M. Haeffelin[6]

[1]IMAA-CNR, Potenza, Italy
[2]CETEMPS, University of L'Aquila, L'Aquila, Italy
[3]Institut Pierre-Simon Laplace, Université Versailles Saint Quentin, Guyancourt, France
[4]Laboratoire de Météorologie Dynamique (LMD), CNRS-Ecole Polytechnique, Palaiseau, France
[5]Department of Environmental Sciences, University of Virginia, Charlottesville, VA, USA
[6]Institut Pierre-Simon Laplace, Centre National de la Recherche Scientifique, Ecole Polytechnique, Palaiseau, France

Abstract

The mixing layer height (MLH) is a key parameter for boundary layer studies, including meteorology, air quality, and climate. MLH estimates are inferred from in situ radiosonde measurements or remote sensing observations from instruments like lidar, wind profiling radar, or sodar. Methods used to estimate MLH from radiosonde profiles are also used with atmospheric temperature and humidity profiles retrieved by microwave radiometers (MWR). This paper proposes an alternative approach to estimate MLH from MWR data, based on direct observations (brightness temperatures, Tb) instead of retrieved profiles. To our knowledge, MLH estimates directly from Tb observations has never been attempted before. The method consists of a multivariate linear regression trained with an a priori set of collocated MWR Tb observations (multi-frequency and multi-angle) and MLH estimates from a state-of-the-art lidar system. Results show that the method is able to follow both the diurnal cycle and the day-to-day variability as suggested by the lidar measurements, and also it can detect low MLH values that are below the full overlap limit (~ 200 m) of the lidar system used. Statistics of the comparison between MWR- and reference lidar-based MLH retrievals show mean difference within 10 m, RMS within 340 m, and correlation coefficient higher than 0.77. Monthly mean analysis for day-time MLH from MWR, lidar, and radiosonde shows consistent seasonal variability, peaking at ~ 1200–1400 m in June and decreasing down to ~ 600 m in October. Conversely, night-time monthly mean MLH from all methods are within 300–500 m without any significant seasonal variability. The proposed method provides results that are more consistent with radiosonde estimates than MLH estimates from MWR retrieved profiles. MLH monthly mean values agree well within 1 std with bulk Richardson number method applied at radiosonde profiles at 11:00 and 23:00 UTC. The method described herewith operates continuously and it is expected to work with analogous performances for the entire diurnal cycle, except during considerable precipitation, demonstrating new potential for atmospheric observation by ground-based microwave radiometry.

1   Introduction

The atmosphere boundary layer is characterized by turbulent fluctuations that induce mixing of aerosol particles and other trace gases and govern vertical distribution of thermodynamic variables. During daytime the lower layers tend to be unstable as a result of surface heating and the boundary layer tend to be neutrally stratified due to the thermally driven convection. At night a shallow stable layer forms near the surface in which mixing occurs primarily through intermittent turbulence, leaving a residual layer above (Stull, 1988). The mixing layer height (MLH) defines the top of the layer near the surface where mixing is occurring. The MLH is a key parameter for boundary layer applications, including meteorology, weather prediction, air quality, and even climate (Deardorff, 1972; Stull, 1988; Garratt, 1992; Piringer et al., 2007; Pal et al., 2012). For instance, the determination of the MLH is crucial to study exchanges between the surface and the atmosphere. In fact, the way pollutants disperse in the atmosphere largely depend on how the MLH has developed: an unstable convective layer favors the dilution of pollutants while a shallow stable layer favors their trapping near the ground. Here, we adopt the MLH definition of Seibert et al. (2000), as "the height of the layer adjacent to the ground over which pollutants emitted within this layer or entrained into it become vertically dispersed by convection or mechanical turbulence". This definition applies both for daytime, where the MLH is the top of a well mixed layer, and for nighttime, where the MLH is the top of the stable layer in which surface emitted pollutants are mixed through intermittent turbulence.

The mixing layer height can be associated to features in the vertical gradients of atmospheric constituents or thermodynamical structure. The vertical information may be obtained either with in situ measurements such as radiosondes, or ground-based observations from remote sensing instruments like light detection and ranging (lidar), sonic detection and ranging (sodar), or wind profiling radar. For example, several approaches are reported till date to estimate MLH using wind profiler radar signal (Bianco and Wilczak, 2002; Bianco et al., 2008), lidar backscatter signal (Baars et al., 2008), or

sodar echo (Beyrich, 1995). A quite comprehensive review of methods for the operational determination of the mixing height is given by Seibert et al. (2000), in which these methods are compared, and strengths and limitations of each method are discussed. For example, MLH is often estimated from the detection of the sharp gradient in the lidar backscatter signal due to aerosol decay at the top of the mixing layer. However, the lidar transreceiver overlap factor causes an offset in the measures of the MLH because stratifications below a certain height, the so called overlap height, cannot be detected (Haeffelin et al., 2012) and so the nocturnal stable boundary layer depth, which is most often shallow. In the recent years, new algorithms have been developed for estimating MLH (Pal et al., 2010; Wang et al., 2012; Granados-Muñoz et al., 2012), though the automatic detection of the top of the mixing layer still remains challenging, especially during shallow stable or nocturnal boundary layer when the mixing layer is not well defined.

Thus, a synergy between different techniques, based on different aspects of the boundary layer, may be explored to improve the MLH estimate around the clock during all meteorological conditions (Praz, 2013). In this perspective, microwave radiometer (MWR) observations can provide a valuable contribution to the determination of the MLH, providing estimates of temperature and humidity in the lower troposphere. Temperature and humidity profiles retrieved by MWR can be used to feed tools developed for estimating MLH from radiosonde temperature and humidity profiles (Seidel et al., 2010), as for example the "parcel method" (Holzworth, 1964; Seibert et al., 2000), and thus providing an independent source of MLH estimates (Wang et al., 2012; Granados-Muñoz et al., 2012; Praz, 2013). In this paper, we present yet another approach based on MWR, where MLH is not inferred from the MWR-retrieved temperature and humidity profiles, but instead estimated directly from MWR observations, i.e. brightness temperatures (Tb). Thus, this approach is independent by the MWR profile retrievals and it is based entirely on the MWR direct observations, Tb. The method is calibrated to the lidar in the sense that it trains the MWR retrieval to identify structures in the Tb that are most consistent with the MLH definition above. The proposed approach brings up

new potential for MWR observations, as to our knowledge MLH estimates directly from Tb observations has never been attempted before. The paper is organized as follows: Sect. 2 presents the data set we used for this analysis; Sect. 3 presents the details of the methodology and the proposed retrieval algorithm; Sect. 4 discusses the results and the validation; Sect. 5 summarises the findings and draws the final conclusions.

2   Data set

The data set considered here was collected at the Site Instrumental de Recherche par Télédétection Atmosphérique (SIRTA), a French national atmospheric observatory dedicated to cloud and aerosol research (Haeffelin et al., 2005). SIRTA is located at Palaiseau (48.8° N, 2.36° E, 65 m a.s.l.), 20 km south of Paris (France) in a semi-urban environment on a 10 km plateau. Active and passive remote sensing instrumentations are routinely operated at SIRTA, including a multi-channel MWR, a backscatter lidar, and a sonic anemometer, while operational radiosondes are launched twice a day by Météo-France (the French national weather service) from Trappes, 12 km west of SIRTA. The availability of all these nearly colocated instruments allows us to demonstrate the proposed technique. A dataset spanning over more than six months (March–October 2011) is utilized here.

2.1   Radiosonde data

The radiosondes used for the analyses presented are M2K2 and M10 sondes manufactured by MODEM, providing profiles of pressure, temperature, relative humidity, dew point temperature, and horizontal wind at 2 s resolution. Though infrequently (few times per day), radiosoundings remain the de facto standard for upper air monitoring and provide the most accurate information on the vertical structure of the troposphere and lower stratosphere. Two radiosondes per day are launched at 11:00 and 23:00 UTC from the Météo-France site in Trappes; a total of 424 radiosondes is available for this

analysis. The MLH can be inferred from radiosonde profiles with a variety of methods (Seibert et al., 2000; Seidel et al., 2010). In this paper, we compute two MLH estimates for each radiosonde, using the following methods:

- the thermodynamical (PTU) method (relying on temperature and humidity profiles only); this is a combination of the parcel method, for estimating MLH in convective boundary layer, and of the surface-based temperature inversion and the virtual potential temperature gradient methods, for estimating MLH during nocturnal and stable boundary layer

- the bulk Richardson number (Rbn) method (relying on temperature, humidity, and horizontal wind profiles); this evaluates the ratio of convective produced turbulence divided by turbulence generated by wind shear against a critical value, set to 0.22 or 0.33 for day and night radiosondes, respectively (Pratz, 2013).

Although the Rbn method is expected to be more reliable, as it also exploits the information on wind shear, the PTU method is more flexible as it can be applied to standard PTU radiosonde with no wind measurement. For further details on the above methods, see Seibert et al. (2000) and Seidel et al. (2010) and references therein.

2.2   MWR data

The multi-channel MWR deployed at SIRTA is a humidity and temperature microwave profiler (HATPRO) manufactured by Radiometer Physics GmbH (Germany) (Rose et al., 2005). It measures brightness temperatures (Tb) at 14 channels (22.24, 23.04, 23.84, 25.44, 26.24, 27.84, 31.4, 51.26, 52.28, 53.86, 54.94, 56.66, 57.3, 58 GHz) and 7 elevation angles (90, 42, 30, 19, 10, 5, 0°). Tb are calibrated using a combination of noise diode injection and a reference target at ambient temperature. The noise diode effective temperature is determined by observing an external cryogenic target less frequently (three to six months). Atmospheric temperature and humidity profiles, as well as column-integrated water vapour (IWV) and liquid water path (LWP), can be

retrieved from MWR observations using a variety of inversion methods, including multi-variate regression, neural networks, and variational approaches (Solheim et al., 1998; Cimini et al., 2006, 2009). The HATPRO proprietary software provides linear regression, quadratic regression, as well as neural networks (Rose and Czekala, 2010). The HATPRO at SIRTA was set to use the neural networks method, which is trained with thousands of profiles generated from historical data sets of operational radiosondes. Ten years of radiosonde data launched from Trappes were used for the training of the SIRTA HATPRO. The information content of MWR observations on the vertical distribution of atmospheric thermodynamical variables resides in the differential absorption of multi-frequency and multi-angle Tb observations. However, MWR observations inherently present significant redundancy, leaving just a few independent pieces of information about the vertical thermodynamical structure. For temperature profiles most of the information content and the vertical resolution resides in the first 2 km, while for humidity profiles the information is spread along the vertical range but at coarser resolution. For a generic MWR operating in the 20–60 GHz range, Lönhert et al. (2009) showed that the degrees of freedom for signal (DFS), i.e. the number of independent levels that can be retrieved, are as follows: (i) for temperature profiles, DFS depend only slightly on atmospheric conditions, but range from ∼ 2 to 4, respectively for zenith and multi-angle observations; (ii) for humidity profiles, DFS are almost independent on elevation angles, but depend noticeably on the water vapour content (DFS ∼ 1–3 from dry to humid environment). An example of 24 h time series of temperature, water vapour mixing ratio, and virtual potential temperature profiles derived from MWR data is shown in Fig. 1. The temperature shows a clear diurnal variation, with the solar radiation warming up the boundary layer from around 07:00 UTC (09:00 LT) until 19:00 UTC, and the development of a weak inversion layer during the night hours (03:00 to 05:00 UTC). As a consequence, the potential temperature transits from stratified conditions to a well-developed mixing within the convective boundary layer. MWR observations (Tb) and products (IWV, LWP, temperature and humidity profiles) are available

at ∼ 1 min temporal resolution. Currently, a direct estimate of the MLH is not provided by HATPRO (Rose and Czekala, 2010), nor by any other commercial MWR.

2.3 Lidar data

The lidar deployed at SIRTA is a 355 nm ALS450 backscatter lidar developed by Leosphere (France) (Lolli et al., 2011). The MLH is derived from lidar backscattering data using the STRAT2-D algorithm that retrieves the most significant gradients in the profiles using two-dimensional gradient analyses (Morille et al., 2007). Haeffelin et al. (2012) compared MLH estimates from ALS450 observations processed with the STRAT2-D algorithm with MLH values obtained from radiosondes using the bulk Richardson number method (as described in Menut et al., 1999); the statistics they reported for daytime and nighttime are given in Table 1.

The STRAT2-D algorithm provides 4 different layers for each 10 min period: the strongest gradient, the second strongest gradient, the lowest-altitude gradient, and cloud-base height. However, the final attribution to determine which of these 4 retrievals best corresponds to the MLH remains ambiguous. The STRAT2-D algorithm has been recently upgraded (Pal et al., 2013) with an enhanced attribution procedure. Surface sonic anemometer measurements are used to compute heat fluxes and friction velocity. These parameters are then used to derive a Monin–Obukov length and an atmospheric stability index. The times of early morning transition and early evening transition are determined from stability transitions. A variance analysis is performed on the lidar backscatter profiles within each one hour interval to determine the height of maximum turbulence. The transition times and turbulence profiles are then used to determine the STRAT2-D-derived gradient that most likely traces the MLH. The finally attributed MLH estimates is available at ∼ 10 min temporal resolution. An example of 24 h time series of range corrected backscatter profiles measured by the ASL450, as well as the associated MLH derived using STRAT2-D, is shown in Fig. 2. The diurnal cycle is such that the aerosols are concentrated in the lower levels during the nighttime stable boundary layer and then are dispersed into a progressively deeper layer as the

convective boundary layer builds up. In the early evening transition period, when solar surface heating stops, a new shallow mixing layer develops near the surface.

3 Methodology

Temperature and humidity profiles retrieved by MWR every ~ 1 min may be used to feed the tools developed for inferring MLH from radiosonde temperature and humidity profiles (Seidel et al., 2010). However, as for radiosonde, the estimated MLH would depend on the different definition that is applied. In addition, the vertical resolution of MWR profiles is much lower than that provided by radiosondes, and the MLH estimate would be affected by that. Therefore, here we propose a different approach, that is a "direct" MLH estimate from Tb measurements. In fact, MLH can be estimated directly from Tb by investigating the covariance of these geophysical variables, provided that an independent "reference" observation for MLH is available for training. This approach offers the following advantages: (i) it is independent from uncorrelated retrieval errors in MWR temperature and humidity profiling, and (ii) it exploits all the DFS provided by the MWR observations for the retrieval of a scalar quantity, i.e. MLH. Despite these advantages, to our knowledge direct MLH estimates from Tb observations has never been attempted before.

Here we adopt a general notation to derive information on the atmospheric state vector x, from the observation vector y, which in our case represents MLH and Tb, respectively. The inverse problem R of estimating x from y, i.e. a finite number of highly correlated observations affected by measurement error ε, can be written as:

$$\widehat{x} = R(y + \varepsilon) \tag{1}$$

which represents an ill-posed problem and thus it accepts non-unique solutions. In the case an a priori dataset of simultaneous state vectors x and observations y is available, it is possible to solve Eq. (1) through empirical regression. In the assumption

of moderate non-linear problem, the solution can be linearized by means of first-order Taylor expansion (calling x_0 and y_0 the mean state and observation vectors):

$$\widehat{x} = x_0 + \mathbf{C}_{xy}\mathbf{C}_{yy}^{-1}(y - y_0) \tag{2}$$

where $\mathbf{C}_{xy}$ and $\mathbf{C}_{yy}$ are extracted from the a priori dataset and represent respectively the covariance matrix of the state vector x and the simultaneous observations y, and the autocovariance matrix of y. In our approach, the observation vector y consists in the HATPRO Tb measurements, while the state vector consists in MLH estimates, as derived for example from radiosonde or lidar data. We prefer the lidar because it provides a much larger data set (every ~ 10 min) covering the complete diurnal cycle, as opposite to twice-daily radiosondes. Therefore, we exploit the a priori dataset of more than six months of colocated ALS450 lidar and HATPRO MWR data at SIRTA to train a multivariate regression as above. In particular, we define as:

  – The state vector x: MLH (m) estimated by lidar backscattering with the upgraded STRAT2-D algorithm (Pal et al., 2013).

  – The observation vector y: multi-channel and multi-angle Tb (K) measured by MWR at all 14 channels and 6 elevation angles (90, 42, 30, 19, 10, 5°). Observations at 0° elevation were not utilized to avoid antenna side-lobe ground contamination.

Temporal co-location is obtained by averaging x and y in 10 min bins for the period May to October 2011, while only for March 2011 data are available in 5 min bins, due to intensive observations during a field campaign dedicated to fog investigation. The entire dataset of 22287 colocations (2931 in March 19356 in May–October) is divided in two independent sub-sets, one for training the regression coefficients while the other for testing the retrieval performances. The training assumed STRAT2-D MLH estimates as the reference "truth" and was performed separately for each month to account for seasonal variations. Moreover, training is performed separately for night- and day-time,

in order to separate convective and stable regimes. The transition between day and night relies on local time; following the results in Pal et al. (2013), here we adopted 11:00 LT as the time for mean morning transition and 19:00 LT for the mean evening transition in June, July, August and September, while 12:00 and 18:00 LT, respectively for morning and evening transitions, in March, May, and October. Therefore, 14 sets of coefficients (7 months times 2 day-night shifts) are determined, and the procedure picks alternatively each one to retrieve MLH from MWR Tb observations according to local date and time only.

4 Results

Following the procedure described above, MLH are estimated from MWR Tb observations for the test set (i.e. not used for training) extracted from the entire data set spanning from March to October 2011. Hereafter the altitude is expressed above ground level (a.g.l.). The results are presented in Fig. 3, together with the reference truth, i.e. the MLH estimated from lidar backscatter by the upgraded STRAT2-D algorithm. It is important to keep in mind that lidar and MWR rely on different aspects of the boundary layer to estimate MLH, the first being based on aerosol distribution while the second on thermodynamical properties. It is evident that the MWR-based MLH estimate is able to follow both the diurnal cycle and the day-by-day variability indicated by the lidar-based estimates. However, discrepancies are also evident, especially at low MLH values, where the MWR-based estimates go often lower than the corresponding lidar-based estimate. This behaviour is consistent with the results in Wang et al. (2012), which conclude that lidar data under weak convection conditions reveal higher MLH values than those estimated from MWR profiles. Additionally, note that, due to the so called lidar overlap limit, the lowest altitude of significant gradient detection is estimated at ~ 200 m for the ALS450 (Haeffelin et al., 2012). However, lidar system performances have some impact on the optical overlap factor, which is a function of height changing from 0 to 1 (full overlap), and therefore detection below 200 m is possible at times, as

can be seen in Fig. 3 during the first week of March. A way to go around the overlap limitation by sensor synergy for determining the entire diurnal cycle of MLH was exploited by Pal et al. (2012), using lidar data for MLH during daytime only, while ceilometer data for nighttime MLH estimates. Figure 4 shows four shorter time series extending for 2–4 days, together with the MLH estimated from radiosondes with both the PTU and Rbn methods, where few diurnal cycles during different conditions can be appreciated. In particular, low level clouds and fog were observed at the SIRTA site for most of the first days of March (Julian day 60–64), with global downwelling shortwave flux below 300 W m^{-2} at surface, inhibiting the development of a convective boundary layer and causing low MLH values during both day- and night-time. Conversely, the two days between the end of May and the beginning of June were characterized by clear sky and scattered high clouds, with global downwelling shortwave flux up to 1000 W m^{-2} at surface, causing a well developed convective boundary layer between 10:00 and 19:00 UTC. The two extreme situations described above are confirmed by the MLH estimated from radiosondes (both PTU and Rbn methods), though just twice a day (~ 11:00 and 23:00 UTC), and concur to form the mixed situations seen in the time series in mid July and mid October. This last time series shows one case in which the MWR-based MLH estimates are lower then lidar estimates and also are evidently closer to the radiosonde Rbn estimates (at Julian day 293.0). This is interesting because it demonstrates that the proposed algorithm, establishing a linear relationship between Tb and MLH, is able to extrapolate the information provided by the reference lidar estimates to values below the lidar overlap limit. As can be seen in Fig. 3, this situation happen quite often in July–September. These results demonstrate the potential of the MWR-based method, confirming useful complementary information with respect to lidar on shallow boundary layer, which is till date a challenging task for ground-based measurements.

The agreement between MWR- and lidar-based MLH estimates is further quantified in Fig. 5 via correlation analyses. Here we show the scatter plots of MLH estimates for the four 1-month periods in Fig. 3. Each point corresponds to 1 h average, so to reduce

the effects of temporal and spatial collocation of the two instruments (less than five meters apart). The scatter plots confirm that the MWR-based estimate is able to follow the dynamical range spanned by the lidar-based MLH, at least up to 2500 m. Note also that low MLH values tend to form a cluster around 200–250 m, close to the lidar overlap limit. Statistical scores of the MWR- vs. lidar-based MLH comparison are reported in Fig. 4 and summarized in Table 2 for each month. For the considered months, the availability of the MLH estimates range from 70 to 99 % except for May and June (15 and 40 %, respectively), due to the instrumental problems of the lidar system. Indeed, the most significant discrepancies correspond to these two months, most probably due to relative poor sample size and the associated low statistical confidence. Overall, the mean difference is generally small (within 10 m), although it reaches significant values for May–June (up to 86 m). As a consequence, STD and RMS of the differences are almost undistinguishable, ranging from 166 m (March) to nearly 950 m (May). Note that the scatter is at minimum for March, likely due to the double temporal resolution of the original time series (5 min instead of 10 min bins), causing a scatter reduction by a factor of 1.41. The correlation coefficient between the MWR- and lidar-based estimate ranges from 0.42 in May to 0.90 in March. Considering the entire data set (3653 1 h average bins), MD is 4 m, RMS 436 m, and correlation coefficient 0.69. However, if we take the results for the three months (March, August, September) in which we have more than 90 % availability, the MD is within 10 m, the RMS within 340 m, and the correlation coefficient higher than 0.77.

In addition to the diurnal cycle, also the seasonal variability of the MLH is important for many applications like the parameterization of numerical weather prediction, climate, and air quality models. The seasonal variability of the MLH depends on a variety of factors, including location, climatology, and topography of the site under analysis. Figure 6 shows the comparison of diurnal monthly mean MLH as derived from different sources (lidar, MWR Tb, MWR profiles, and radiosondes). The diurnal values are computed averaging all the data falling into 1 h window from the launch time of day-time radiosonde (around 11:30 UTC). Values from both radiosonde methods (PTU and Rbn)

are shown, with the PTU consistently lower than Rbn by 100–200 m. Overall, monthly mean MLH from MWR, lidar and radiosonde agree reasonably well (within 200 m) and show a consistent seasonal variability, peaking in June at ∼ 1200–1400 m and decreasing down to ∼ 600 m in October. The MLH from MWR profiles is consistently lower than every other estimate by 300–600 m, showing a reduced dynamical range for seasonal variability (from 800 m in June down to 450 m in October). Note that the estimates from MWR profiles are obtained with exactly the same method used for the radiosonde estimates (i.e. a combination of parcel, surface based inversion, and potential temperature gradient methods), and thus the differences we see in Fig. 6 between these two estimates are mainly related to the different sensitivity and vertical resolution provided by radiosonde and MWR profiles. Conversely, let us remind that the proposed method relies on a different approach, i.e. MLH estimates from direct MWR Tb observations. The nocturnal monthly mean MLH from the same sources as above is shown in Fig. 7. The nocturnal values are computed averaging all the data falling into 1 h window from the launch time of night-time radiosonde (around 23:30 UTC). The nocturnal monthly mean MLH is significantly lower than diurnal, all the sources indicating values below 500 m and showing no clear seasonal signature. As for the diurnal MLH, the radiosonde PTU is consistently lower than Rbn, though the difference during night is reduced to 10–100 m, while the MLH from MWR profiles is consistently lower than every other estimate by up to 150 m. Nocturnal monthly mean MLH from radiosonde Rbn, lidar, and MWR Tb agree within 100–200 m.

5 Summary and conclusions

This paper demonstrates the potential for estimating MLH directly from MWR Tb observations. The proposed approach is based on a multivariate linear regression trained with an a priori set of nearly colocated and simultaneous MWR Tb observations (multi-frequency, multi-angle) and MLH estimates from state-of-the-art lidar-based method aided with variance and stability index analysis. This approach is alternative to the

MLH estimates from MWR retrieved profiles, which has been used in recent intercomparison studies (Wang et al., 2012; Granados-Muñoz et al., 2012; Pratz, 2013), as it exploits the whole vertical information content provided by the MWR for the retrieval of the scalar quantity MLH. It may be argued that the proposed method needs an a priori set of reference data for training the algorithm, but this is indeed true also for MWR profile retrievals. In fact, the proposed approach could be easily implemented in addition to the implementation of temperature, humidity, IWV, and LWP retrievals, taking the radiosondes as reference.

The results show that MWR-based MLH estimate is able to follow both the diurnal cycle and the day-to-day variability suggested by the lidar-based estimates. Our results also demonstrate that the proposed MWR-based method, although trained with lidar estimates, is able to detect low MLH values that are below the lidar overlap limit (~ 200 m) prevailing during mainly stable boundary layer regimes at night. Comparison between MWR- and reference lidar-based MLH retrievals for a 7-month period (divided into 1 h average bins), shows a small mean difference (4 m), RMS equal to 436 m, and correlation coefficient to 0.69. However, taking into account the results for the three selected months (March, August, September) with more than 90 % data availability, the mean difference is within 10 m, the RMS within 340 m, and the correlation coefficient higher than 0.77.

The analysis of monthly mean MLH showed that during day-time, MWR, lidar and radiosonde Rbn agree within 200 m, showing a consistent seasonal variability, peaking in June at ~ 1200–1400 m and decreasing down to ~ 600 m in October, while estimates from MWR profiles are consitently lower than every other estimate by 300–600 m, showing reduced seasonal variability. During night-time, monthly mean MLH is below 500 m, showing no clear seasonal signature. Estimates from MWR Tb and lidar agree within 200 m with radiosondes Rbn, while estimates from MWR profiles are consitently lower by 150 m. Thus, when compared to MLH estimated from MWR profiles, the proposed method provide results that are more consistent with radiosonde Rbn estimates during both day and night. MLH monthly mean values from the proposed method agree

well within one sigma with radiosonde Rbn estimates at 11:00 and 23:00 UTC, while MLH estimates from MWR retrievals are consistently lower by ~ 300–500 m during daytime and ~ 100–200 m during nighttime. Finally, this analysis concurs that the combination of MWR and lidar, as well as other remote and in situ sensing instrumentations, seems crucial for studying the temporal variability in MLH (both diurnal and seasonal). A synergetic approach, considering different techniques based on different aspects of the boundary layer, shall be explored to improve the MLH estimate during all stability conditions using further longer-term measurements at SIRTA atmospheric observatory.

References

Baars, H., Ansmann, A., Engelmann, R., and Althausen, D.: Continuous monitoring of the boundary-layer top with lidar, Atmos. Chem. Phys., 8, 7281–7296, doi:10.5194/acp-8-7281-2008, 2008.

Beyrich, F.: Mixing-height estimation in the convective boundary layer using sodar data, Bound.-Lay. Meteorol., 74, 1–18, 1995.

Bianco, L. and Wilczak, J. M.: Convective boundary layer depth: improved measurement by doppler radar wind profiler using fuzzy logic methods, J. Atmos. Ocean. Tech., 19, 1745–1758, 2002.

Bianco, L., Wilczak, J., and White, A. B.: Convective boundary layer depth estimation from wind profilers: statistical comparison between an automated algorithm and expert estimations, J. Atmos. Ocean. Tech., 25, 1397–1413, 2008.

Cimini, D., Hewison, T. J., Martin, L., Güldner, J., Gaffard, C., and Marzano, F.: Temperature and humidity profile retrievals from groundbased microwave radiometers during TUC, Meteorol. Z., 15, 45–56, 2006.

Cimini, D., Westwater, E. R., and Gasiewski, A. J.: Temperature and humidity profiling in the Arctic using millimeter-wave radiometry and 1-DVAR, IEEE T. Geosci. Remote, 48, 1381–1388, doi:10.1109/TGRS.2009.2030500, 2009.

Deardorff, J. W.: Parametrerization of the planetary boundary layer for use in general circulation models, Mon. Weather Rev., 100, 93–106, 1972.

Garratt, J. R.: The atmospheric boundary layer, Cambridge University Press, Cambridge, 1992.

Granados-Muñoz, M. J., Navas-Guzmán, F., Bravo-Aranda, J. A., Guerrero-Rascado, J. L., Lyamani, H., Fernández-Gálvez, J., and Alados-Arboledas, L.: Automatic determination of the planetary boundary layer height using lidar: one-year analysis over southeastern Spain, J. Geophys. Res., 117, D18208, doi:10.1029/2012JD017524, 2012.

Haeffelin, M., Barthès, L., Bock, O., Boitel, C., Bony, S., Bouniol, D., Chepfer, H., Chiriaco, M., Cuesta, J., Delanoë, J., Drobinski, P., Dufresne, J.-L., Flamant, C., Grall, M., Hodzic, A., Hourdin, F., Lapouge, F., Lemaître, Y., Mathieu, A., Morille, Y., Naud, C., Noël, V., O'Hirok, W., Pelon, J., Pietras, C., Protat, A., Romand, B., Scialom, G., and Vautard, R.: SIRTA, a ground-based atmospheric observatory for cloud and aerosol research, Ann. Geophys., 23, 253–275, doi:10.5194/angeo-23-253-2005, 2005.

Haeffelin, M., Angelini, F., Morille, Y., Martucci, G., Frey, S., Gobbi, G. P., Lolli, S., O'Dowd, C. D., Sauvage, L., Xueref-Rémy, I., Wastine, B., and Feist, D. G.: Evaluation of mixing-height retrievals from automatic profiling lidars and ceilometers in view of future integrated networks in Europe, Bound.-Lay. Meteorol., 143, 49–75, doi:10.1007/s10546-011-9643-z, 2012.

Holzworth, G. C.: Estimates of mean maximum mixing depths in the contiguous United States, Mon. Weather Rev., 92, 235–242, 1964.

Löhnert, U., Turner, D., and Crewell, S.: Ground-based temperature and humidity profiling using spectral infrared and microwave observations, Part 1: Simulated retrieval performance in clear-sky conditions, J. Appl. Meteorol. Clim., 48, 1017–1032, 2009.

Lolli, S., Sauvage, L., Loaec, S., and Lardier, M.: EZ Lidar: a new compact autonomous eye-safe scanning aerosol Lidar for extinction measurements and PBL height detection, validation of the performances against other instruments and intercomparison campaigns, Óptica Pura y Aplicada, 44, 33–41, 2011.

Menut, L., Flamant, C., Pelon, J., and Flamant, P. H.: Urban boundary-layer height determination from lidar measurements over the Paris area, Appl. Optics, 38, 945–954, 1999.

Morille, Y., Haeffelin, M., Drobinski, P., and Pelon, J.: STRAT: an automated algorithm to retrieve the vertical structure of the atmosphere from single-channel lidar data, J. Atmos. Ocean. Tech., 24, 761–775, 2007.

Pal, S., Behrendt, A., and Wulfmeyer, V.: Elastic-backscatter-lidar-based characterization of the convective boundary layer and investigation of related statistics, Ann. Geophys., 28, 825–847, doi:10.5194/angeo-28-825-2010, 2010.

Pal, S., Xueref-Remy, I., Ammoura, L., Chazette, P., Gibert, F., Royera, P., Dieudonné, E., Dupont, J.-C., Haeffelin, M., Lac, C., Lopez, M., Morille, Y., and Ravettad, F.: Spatio-temporal variability of the atmospheric boundary layer depth over the Paris agglomeration: an assessment of the impact of the urban heat island intensity, Atmos. Environ., 63, 261–275, 2012.

Pal, S., Haeffelin, M., and Batchvarova, E.: Exploring a geophysical process-based attribution technique for the determination of the atmospheric boundary layer depth using aerosol lidar and near surface meteorological measurements, J. Geophys. Res.-Atmos., under review, 2013.

Piringer, M., Joffre, S., Baklanov, A., Christen, A., Deserti, M., Ridder, K., Emeis, S., Mestayer, P., Tombrou, M., Middleton, D., Baumann-Stanzer, K., Dandou, A., Karppinen, A., and Burzynski, J.: The surface energy balance and the mixing height in urban areas – activities and recommendations of COST-Action 715, Bound.-Lay. Meteorol., 124, 3–24, 2007.

Praz, C.: Automatic planetary boundary layer detection: validation of various detection instruments and methods, comparison with the forecast model Cosmo-2 and one-year climatology, MeteoSwiss-EPFL Internship Report, January 2013.

Rose, T., Crewell, S., Löhnert, U., and Simmer, C.: A network suitable microwave radiometer for operational monitoring of the cloudy atmosphere, Atmos. Res., 75, 183–200, 2005.

Rose, Th. and Czekala, H.: RPG's Atmospheric Remote Sensing Radiometers – Operating Manual, Version 8.12, August 2010.

Seibert, P., Beyrich, F., Gryning, S. E., Joffre, S., Rasmussen, A., and Tercier, P.: Review and intercomparison of operational methods for the determination of the mixing height, Atmos. Environ., 34, 1001–1027, 2000.

Seidel, D. J., Ao, C. O., and Li, K.: Estimating climatological planetary boundary layer heights from radiosonde observations: comparison of methods and uncertainty analysis, J. Geophys. Res., 115, D16113, doi:10.1029/2009JD013680, 2010.

Solheim, F., Godwin, J., Westwater, E., Han, Y., Keihm, S., Marsh, K., and Ware, R.: Radiometric profiling of temperature, water vapor, and cloud liquid water using various inversion methods, Rad. Sci., 33, 393–404, 1998.

Stull, R. B.: An Introduction to Boundary Layer Meteorology, Kluwer Academic Publishers, Dordrecht/Boston/London, 1988.

Wang, Z., Cao, X., Zhang, L., Notholt, J., Zhou, B., Liu, R., and Zhang, B.: Lidar measurement of planetary boundary layer height and comparison with microwave profiling radiometer observation, Atmos. Meas. Tech., 5, 1965–1972, doi:10.5194/amt-5-1965-2012, 2012.

Table 1. Statistics for the comparison between MLH estimated from lidar and radiosonde observations (adapted from Haeffelin et al., 2012). The mean difference (MD), standard deviation (STD), and correlation coefficient (CC) are reported. A total of 53 radiosondes were used.

Period	MD (m)	STD (m)	CC
Daytime	−130	345	0.73
Nighttime	−160	712	0.29

Table 2. Statistics for the comparison between MLH estimated by MWR and lidar observations. The 1 h bin sample size (SS), the mean difference (MD), the standard deviation (STD), the root-mean-square (RMS), and the correlation coefficient (CC) are reported.

Period	Sample Size	MD (m)	STD (m)	RMS (m)	CC
Mar	718	−0.76	166.57	166.57	0.90
May	105	−86.09	944.35	948.35	0.42
Jun	289	84.93	761.13	765.87	0.53
Jul	606	−26.06	588.07	588.65	0.68
Aug	743	−10.77	225.34	225.59	0.89
Sep	671	−7.69	340.00	340.08	0.77
Oct	507	6.99	381.77	381.83	0.52
All data	3653	−3.64	435.75	435.76	0.69
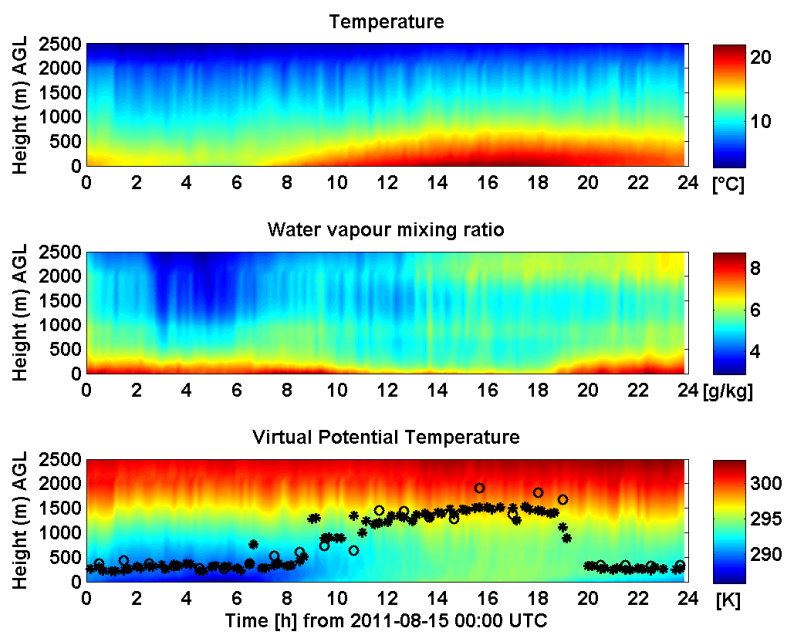
Fig. 1. 24 h time-height cross section of (top) temperature, (middle) water vapour mixing ratio, and (bottom) virtual potential temperature as derived from HATPRO MWR data collected at SIRTA on 15 August 2011. Black stars and circles indicate the MLH estimates from lidar and MWR data, respectively, as discussed in Sect. 3.
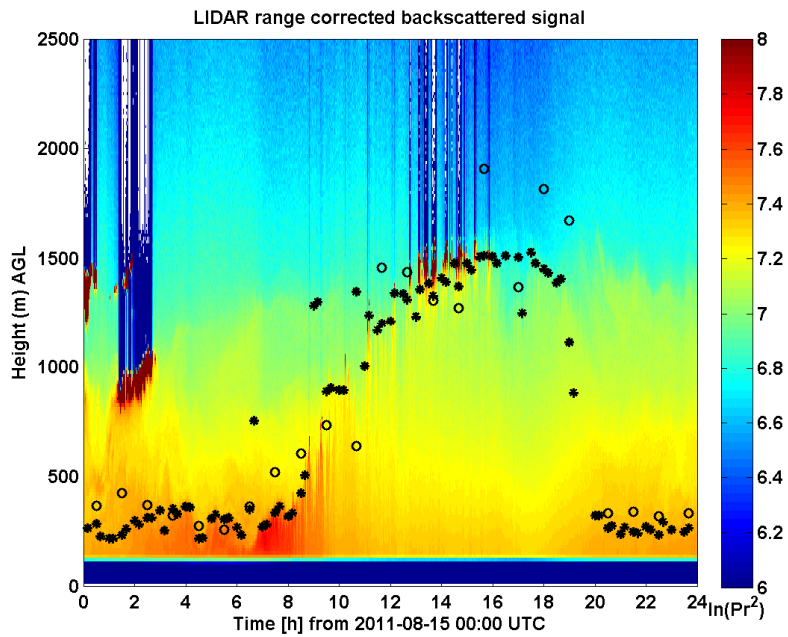
Fig. 2. 24 h time-height cross section of range corrected backscattered signal as measured by the ALS450 lidar at SIRTA on 15 August 2011. Black stars and circles indicate the MLH estimates from lidar and MWR data, respectively, as discussed in Sect. 3.
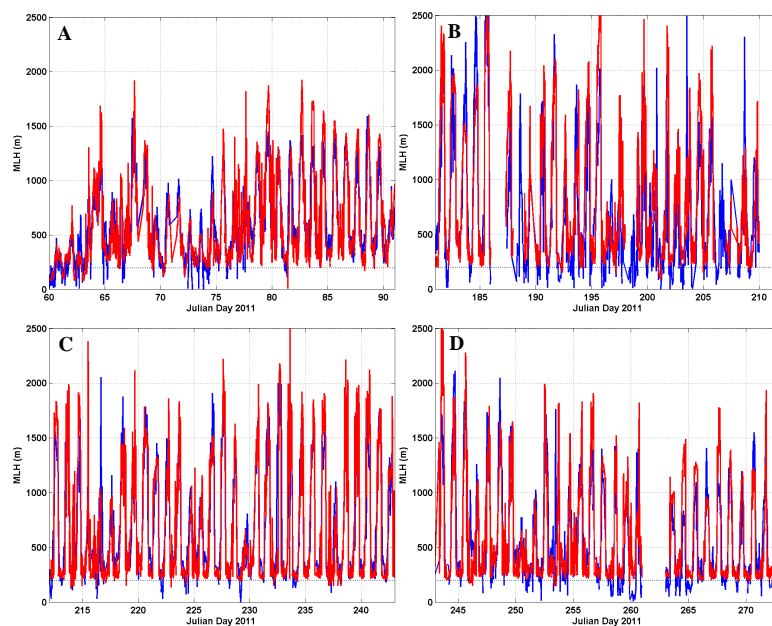
Fig. 3. Time series of MLH (in m a.g.l.) estimated from lidar backscatter (red line) and MWR Tb (blue line) observations. Time is expressed in Julian day (day of the year). The four panels indicate March **(A)**, July **(B)**, August **(C)**, and September **(D)** 2011. The dashed lines at 200 m indicate the lidar full overlap height for the ALS450.
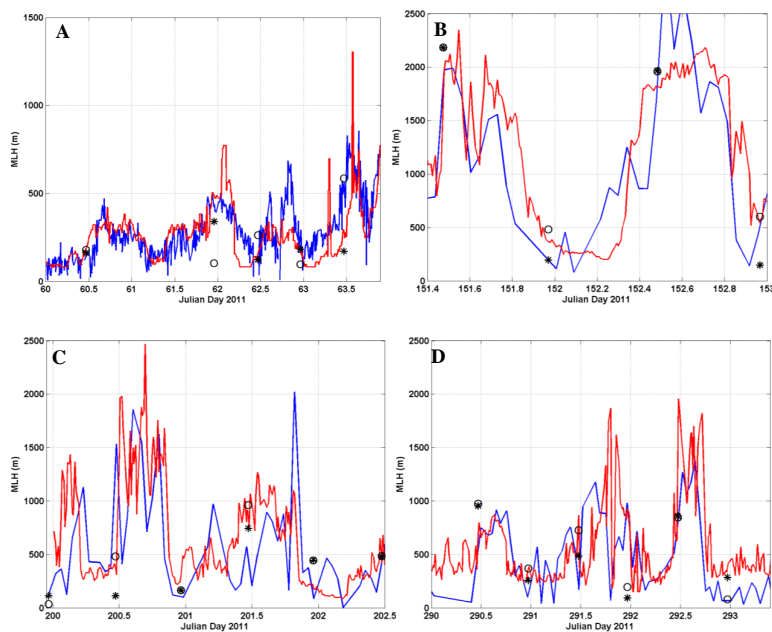
Fig. 4. Short time series of MLH (m a.g.l.) estimated from radiosonde profiles (black stars and circles indicating PTU and Rbn, respectively), lidar (red line) and MWR Tb (blue) observations. **(A)**: (60.0–63.5) corresponds to (1 March 00:00 UTC–4 March 12:00 UTC); **(B)**: (151.4–153.0) corresponds to (31 May 09:36 UTC–2 June 00:00 UTC); **(C)**: (200.0–202.5) corresponds to (19 July 00:00 UTC–22 July 12:00 UTC); **(D)**: (290.0–293.5) corresponds to (17 October 00:00 UTC–20 October 12:00 UTC).
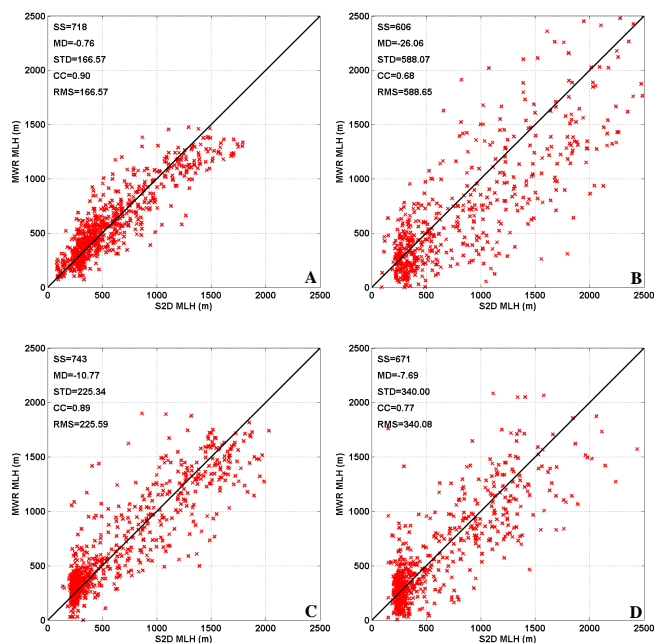
Fig. 5. Scatter plots of MLH (m a.g.l.) estimated from MWR (Y axis) and lidar (X axis) observations. Each panel reports the 1 h average bin sample size (SS), the mean difference (MD), the standard deviation (STD), the root-mean-square (RMS), and finally the correlation coefficient (CC), together with the diagonal 1 : 1 bisector line (black bold). The four panels indicate March **(A)**, July **(B)**, August **(C)**, and September **(D)** 2011.
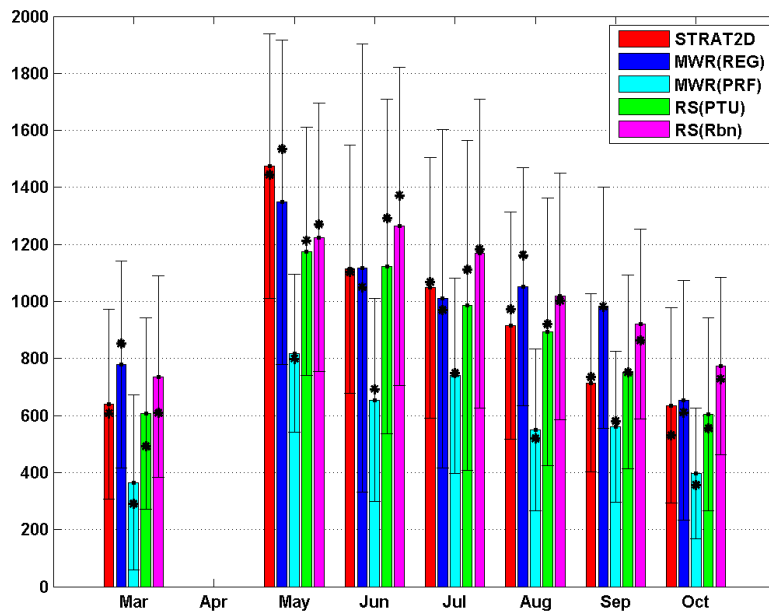
Fig. 6. Monthly mean average of diurnal MLH (m a.g.l.) as estimated by STRAT2-D (red), MWR Tb regression (blue), MWR profiles (cyan), radiosonde PTU (green), and radiosonde Rbn (magenta). Black stars and error bars indicate the median value and one standard deviation, respectively. Values are taken as 1 h average around 11:30 UTC.
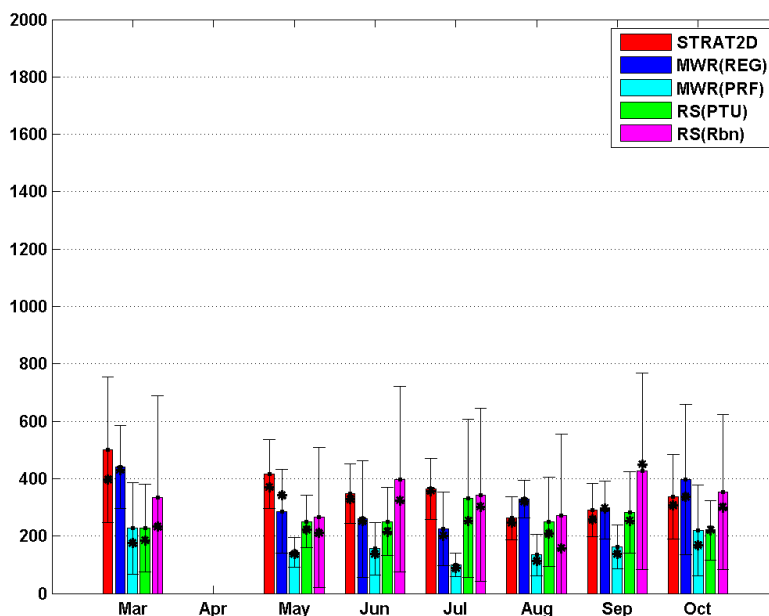
Fig. 7. As in Fig. 6 but for nocturnal MLH (m a.g.l.). Values are taken as 1 h average around 23:30 UTC.